Comparison of polarimetric radar signatures in hailstorms simultaneously observed by C-band and S-band radars.

R. Kaltenboeck[1] and A. Ryzhkov[2]

[1]*Austrocontrol - Aviation Weather Service, Vienna and Institute of Meteorology and Geophysics, University of Innsbruck, Austria, rudolf.kaltenboeck@austrocontrol.at*

[2] *Cooperative Institute for Mesoscale Meteorological Studies, Atmospheric Radar Research Center, University of Oklahoma and National Severe Storms Laboratory, NOAA, Norman, OK, USA, alexander.ryzhkov@noaa.gov*

(Dated: 16 May 2012)

1. Introduction

Direct comparisons of polarimetric signatures in hailstorms simultaneously observed by C-band and S-band radars in Oklahoma reveal numerous differences. Vertical profiles of radar reflectivity Z_H, differential reflectivity Z_{DR}, and cross-correlation coefficient ρ_{hv} in the major downdraft cores of hailstorms at S and C bands reflect fundamental differences in backscattering by melting hailstones and large raindrops at the two wavelengths (e.g. Kaltenboeck and Ryzhkov 2012).

The focus of this study is to examine the signatures at the periphery of the major reflectivity cores which are affected by strong size sorting (Kumjian and Ryzhkov 2009), three-body scattering (TBSS, Lemon 1998), attenuation (Borowska et al. 2011), updrafts (e.g., Straka et al. 2000), side lobe contamination, nonuniform beam filling and reflectivity gradients across the beam (Ryzhkov 2007), depolarization (Ryzhkov and Zrnić 2007), low signal to noise ratio (SNR), and range dependency which manifest themselves very differently at S and C bands. Some of these factors are closely associated with hail itself and its size and their comparative analysis may provide additional insight into the microphysics of hail generation and fallout.

2. Data

Over a period of 3 years, different SPC hail size reports were analyzed in association with data from two polarimetric weather radars closely located in Norman, Oklahoma. One of them is the polarimetric prototype of the WSR-88D S-band radar (KOUN) operated by NOAA (NSSL/ROC) and another one is the C-band OU-PRIME radar operated and maintained by ARRC / University of Oklahoma.

3. Vertical profiles of radar variables in hail.

Typical vertical profiles of radar variables observed in hail are shown in Fig.1.

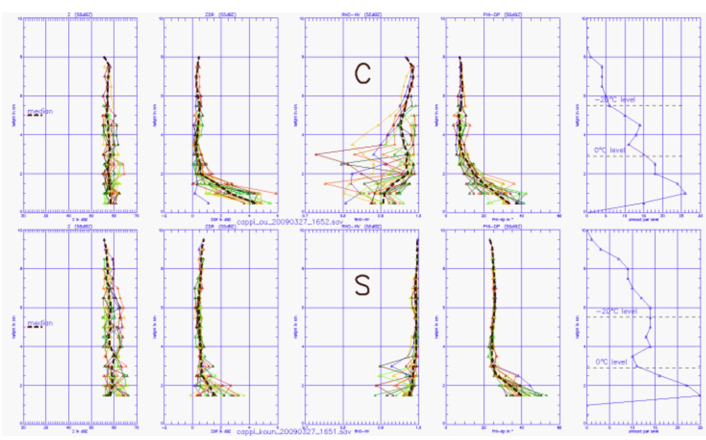

Fig.1: Vertical profiles of polarimetric variables ($Z_H \geq 55$ dBZ) in hail bearing cell. Reported hail size is 2.5 cm. Upper panel shows C-band data and lower panel shows S-band data respectively. From left to right: Z_H, Z_{DR}, ρ_{hv}, ϕ_{DP}, and counts per level. Vertical profiles reveal stronger scattering of Z_{DR} /ρ_{hv} data at C band at different levels. Median vertical profiles are plotted in black.

Below freezing level, stronger increase of positive Z_{DR} and decrease of ρ_{hv} at C band indicate melting hail with resonance sizes. The secondary ρ_{hv} minimum is observed in the wet growth region aloft which is more pronounced at C band for large or giant hail. Polarimetric variables such as Z_{DR}, ρ_{hv} and ϕ_{DP} (differential phase) are more scattered at C band than at S band which is caused by resonance effects and strong differential attenuation. Subsequently, the standard deviations (STD) of polarimetric moments within high reflectivity cell cores are much larger at C than at S band. Larger STD below freezing level for Z_{DR} / ρ_{hv} and for ρ_{hv} aloft at the wet growth regime can be possibly used for hail size discrimination (Kaltenboeck and Ryzhkov 2012).

4. Secondary polarimetric signatures associated with hail.

The following section presents a collection of secondary polarimetric attributes of hail which can affect hail detection, determination of its size, and vertical profiles of polarimetric variables within or close to the convective core containing hail. These effects are more pronounced at C band due to stronger effects of resonance scattering and attenuation. Most of these effects depend on relative positions of the storm and the radar. These secondary signatures can be both beneficial and detrimental for appropriate hail identification. These signatures were identified in the process of visual inspection of radar data collected over 3 year period of observations.

4.1 Hail spike and side lobe effects

Fig.2a illustrates the TBSS and side lobe effects for the storm producing 2.5 cm hail at C and S bands at two PPI elevations. The three-body scattering signature (TBSS) is indicated by a radial spike of moderate Z_H behind cell core. The spike is characterized by positive Z_{DR} close to core followed by negative Z_{DR} further away from the core and low values of ρ_{hv}. The three-body scattering is more apparent in terms of polarimetric variables and the Z_{DR} dependence on range is explained in Picca and Ryzhkov (2012). At elevation 6°, the TBSS signature is more pronounced at C band which might indicate stronger contributions of resonant scatterers.

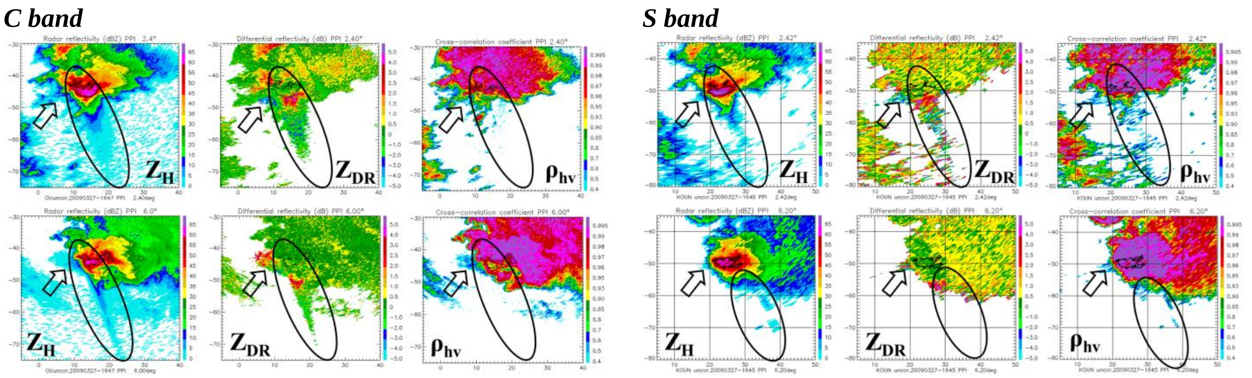

Fig.2a: Hail Spike (TBSS) and side lobe effects seen at PPI elevations of 2.4° and 6.2° (top and bottom panels respectively) on 27th March 2009 at 16:47/45 UTC for the storm producing 2.5cm hail. TBSS is marked by black ellipse, side lobe effects tangential to the cell core are indicated by black arrow. While C-band TBSS and side lobe effects are more pronounced at 6°, the S-band data show more pronounced feature at lower level at 2.4 ° (upper panel).

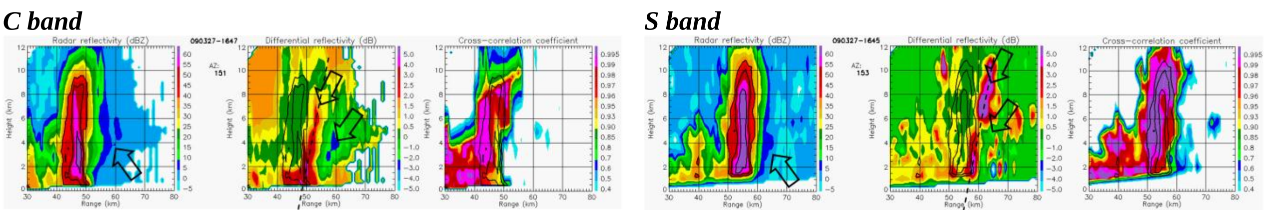

Fig.2b: RHI at azimuth 151 and 153° respectively. TBSS is marked by black arrow in Z_H panel. RHI is given to illustrate tilted Z_{DR} signature (dashed black line) originated from TBSS and left of this signature a Z_{DR}-hole structure aloft can be found. Negative Z_{DR} caused by TBSS at 4 km height is marked with black arrow.

Additional RHIs (Fig.2b) for C-band data are shown to reveal differences in vertical structure of radar variables. The Z_{DR} depression (marked by arrow) appears tilted due to the geometry of TBSS. Longer propagation path of radiation reflected from the ground projects into larger apparent TBSS distances from the radar at higher elevations. Note the Z_{DR}-hole with values close to 0 dB which indicates large hail aloft. Weak echo at the periphery of the cell core is attributed to side lobe effects (marked by an arrow) associated with low ρ_{hv} and noisy, mostly positive Z_{DR}.

4.2 Z_{DR} column

Cross section in Fig.3 shows Z_{DR} column associated with updraft in the bounded weak echo region (BWER) next to precipitation core with high values of Z_H. . The Z_{DR} column develops when large raindrops are lifted above the freezing level. It usually precedes subsequent development of hail. In this example, the Z_{DR} columns are well developed at C and S band and Z_{DR} values as high as 2.5 dBZ are observed at 6 km height (about -20 °C) and accompanied by the decrease of ρ_{hv}. Notable are negative values of Z_{DR} at the base of the Z_{DR} column at C band which is a result of strong differential attenuation in the main precipitation core.

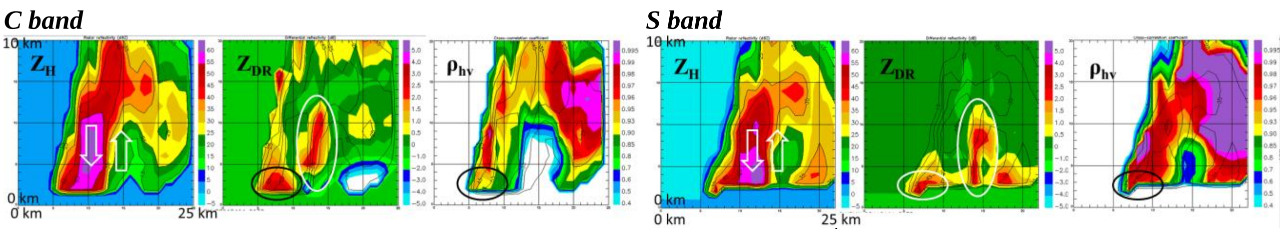

Fig.3: Cross section from NW-SE through 10.8 cm hail-bearing supercell from 14th April 2011 2132+2130UTC showing Z_{DR} column (marked) which indicates the updraft position within BWER. Large melting hail causing high Z_{DR} (low ρ_{hv}) values close to the surface marked as white (black) ellipse. Wet bulb freezing level for that day was 2520 m msl.

4.3 Z_{DR} arc and strong C-band attenuation

Fig. 4 illustrates Z_{DR} arc which is very visible in the southern part of the rear-flank downdraft at S band but is not detectable at C band due to strong differential attenuation. As expected, in the part of the storm facing the radar, $Z_{DR}(C) > Z_{DR}(S)$ due to resonance scattering. In the shadow of the storm (with respect to the radar), differential attenuation at C band is overwhelming and the C-band cross-correlation coefficient is significantly reduced due to stronger impact of nonuniform beam filling at C band.

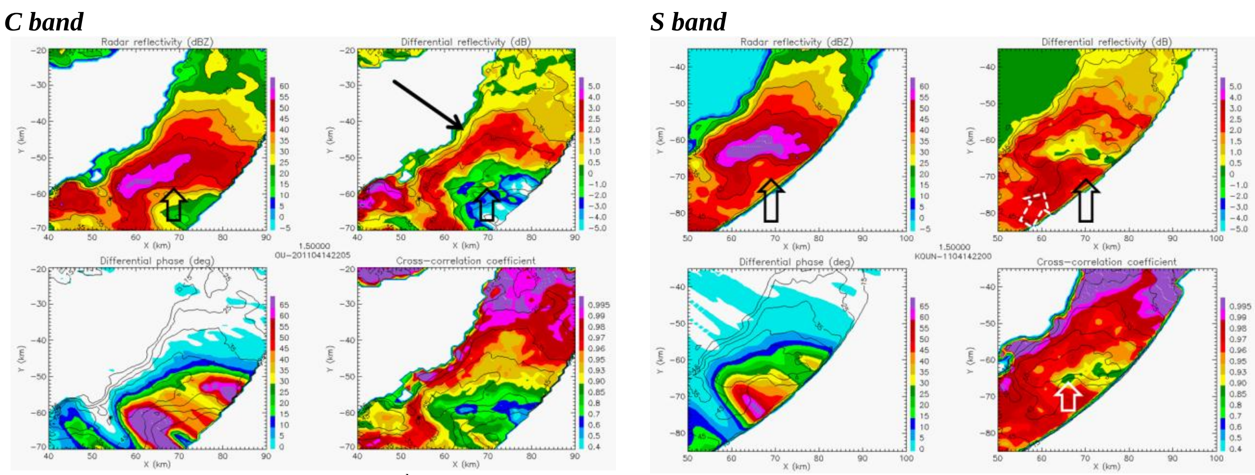

Fig.4: CAPPI at 1.5 km height from 14th April 2011 2205+2200 UTC (4.4 cm hail report) for Z_H, Z_{DR}, Φ_{DP} and ρ_{hv}. C-band polarimetric variables are strongly affected by attenuation and nonuniform beam filling. S-band data show more clearly Z_{DR} arc (black arrow) and Z_{DR} column (marked by white dashed arrow).

4.4 Low SNR and C-band attenuation

Effects of nonuniform beam filling are demonstrated in Fig.5 and 6 which show strong gradients of $Z_{H,}$ Z_{DR} (negative C-band Z_{DR} values behind the core), and Φ_{DP}. The latter causes strong reduction of ρ_{hv}. The SNR dropped down at the outer edge of the storm. White arrow in Fig.5 marks the Z_{DR}-circle structure NE of cell core which is pronounced in C- and S-band data (up to 4 dB). Below freezing level (wet bulb freezing level at 2760 m msl), this might be a graupel belt wrapping around the storm core as an embryo corridor including entrainment and melting. This curved structure also might indicate mesoscale rotation.

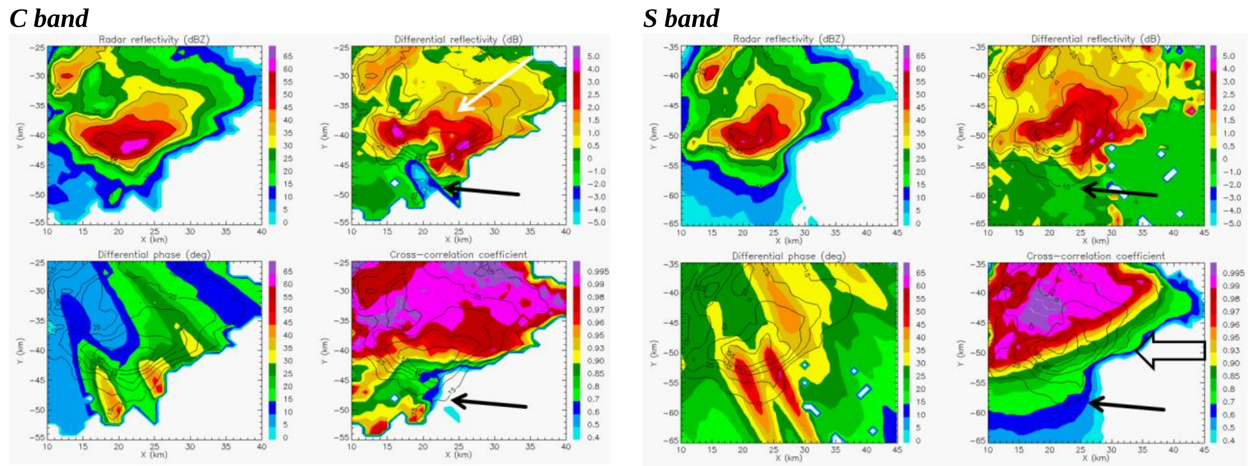

Fig.5: Strong Z_H and Z_{DR} gradients (negative $Z_{DR}(C)$ due to differential attenuation marked by black arrow) resulting low ρ_{hv} and strong decrease of SNR behind cell core seen at lowest CAPPI level 1.5 km GND from 27th March 2009 16:47+45 UTC for 2.5cm hail report. Left (right) panel show C (S) band including subplots of Z_H, Z_{DR} and Φ_{DP}, ρ_{hv}. White filled arrow denotes the decrease of ρ_{hv} due to low SNR at southern flank, while white arrow mark the ZDR-circ at C band.

4.5 Nonuniform beam filling / Φ_{DP} gradient.

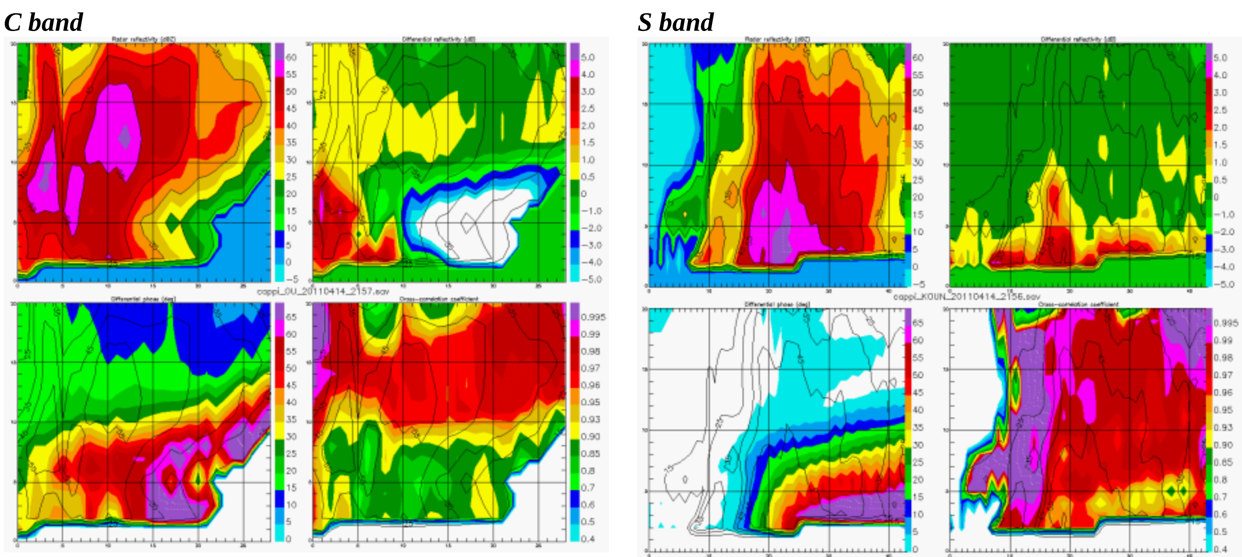

Fig.6: As Fig. 4 except cross section from SW-NE through 2.5 cm hail bearing cell along ray from 14th April 2011 21:56 UTC and negative $Z_{DR}(C)$ behind cell core. Φ_{DP} gradient results in low ρ_{hv}.

4.6 Z_{DR}-circle

Same Z_{DR}-circle pattern as in Fig.5 (northeast of cell core) was observed at the western flank of the storm (Fig.7). The feature is more pronounced at C than at S band. The position of the Z_{DR}-circle might be related to low level inflow and development of flanking line updraft turrets. Soundings from Oklahoma for these days reveal low level winds from NE for Fig.5 (northern flank Z_{DR}-circle) and from SE-SW for Fig.7 (western flank Z_{DR}-circle). More pronounced Z_{DR}-circle (at C band) occurs for the 4.4 cm than for the 10.8 cm hail case.

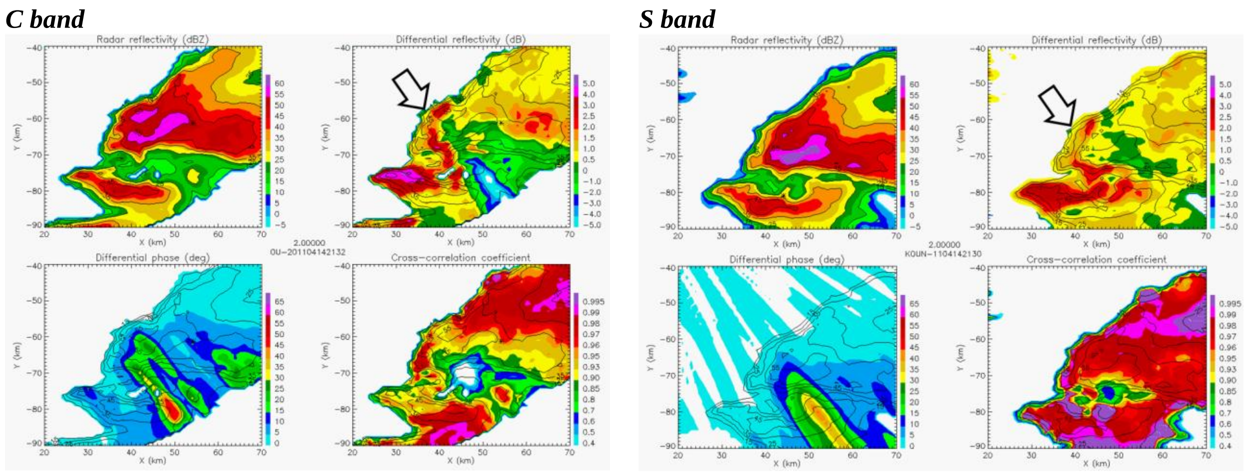

Fig.7: As Fig.5 except CAPPI level at 2 km which show semi Z_{DR}-circle (marked by arrow) for 10.8 cm hail size case from 14th April 2011 2130 UTC. The Z_{DR}-circle at lower levels is more pronounced in C-band.

4.7 Depolarization

Last example shows depolarization pattern which appear as closely located radials of negative and positive Z_{DR} at higher elevations (Fig. 8).

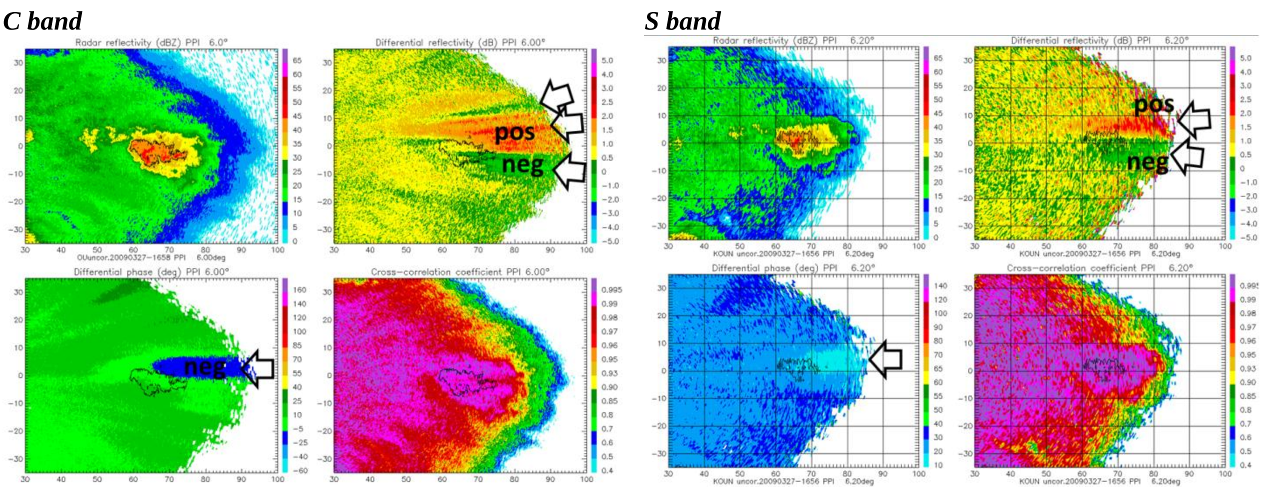

Fig.8a: Z_H, Z_{DR}, Φ_{DP} and ρ_{hv} are shown at PPI elevation 6 and 6.2° at C/S band from 27th March 2009 1658/1656 UTC. Depolarization streaks are marked by the arrows. All plots show overlaid 30 dBZ contour.

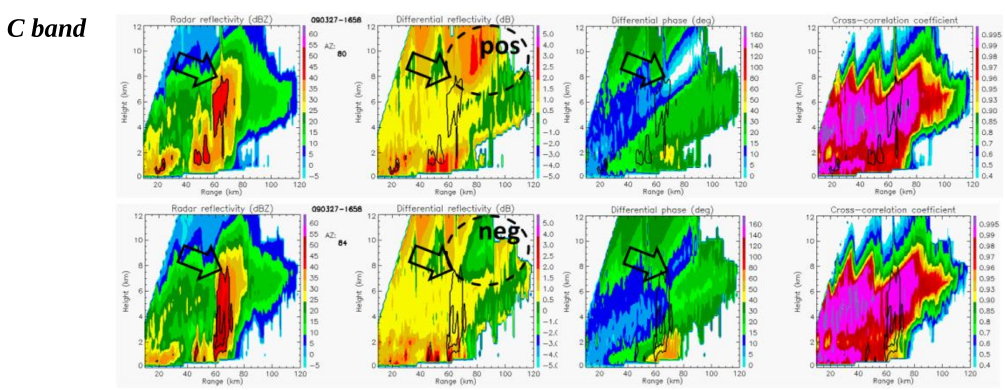

Fig.8b: Upper (lower) panel show RHI of Z_H, Z_{DR}, Φ_{DP}, and ρ_{hv} for azimuths 80 and 84 ° at C band from 27th March 2009 1658 UTC. Depolarization (marked by dashed circle) on top of cell core is seen in the Z_{DR} and Φ_{DP} panels. Starting point of depolarization is marked by arrow.

S band

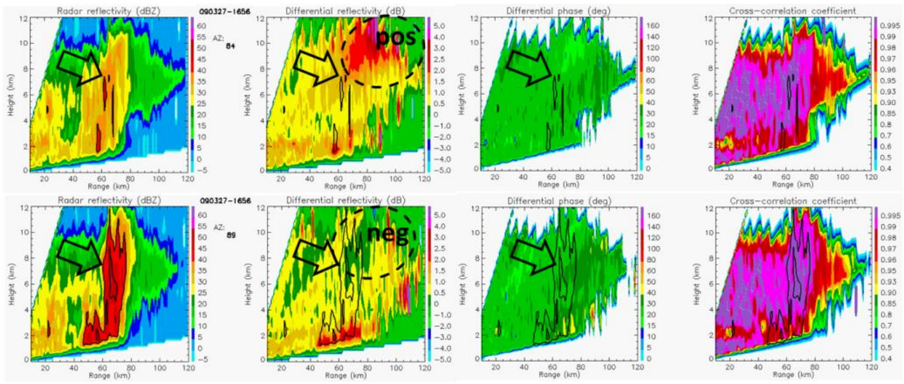

Fig.8c: as Fig.8b except for azimuths 84 and 89 ° at S band.

Those features start on the top of the updraft and are caused by oriented ice crystals due to the electric field within thunderstorm. The PPI and RHI in Fig.8 show sectors of positive and negative Z_{DR} behind storm tops and center (even with high Z_H) which vary in the range of -2 to +3 dB at both wavelengths. The Z_{DR} depolarization streaks are accompanied by negative Φ_{DP} (more pronounced at C band).

5. Conclusion

The polarimetric signatures at the periphery of the major reflectivity hail cores have been examined for 3 years of simultaneously collected C- and S-band data in Oklahoma. These signatures include size sorting manifested as Z_{DR}-arc/rings, TBSS, attenuation, updrafts (Z_{DR}-columns), side lobe contamination, nonuniform beam filling associated with reflectivity gradients across the beam, and depolarization streaks. These secondary polarimetric signatures should be taken into account in the interpretation of radar data and hail detection. Some of them, such as TBSS can be viewed as additional attributes of large hail. Several associated Z_{DR} features (columns, arcs, rings) may indicate imminent development of hail. Enhanced effects of attenuation and nonuniform beam filling at C band may mask the key attributes of hail and can be erroneously qualified as indicators of hail outside of real hail cores.

Acknowledgment

The authors would like to thank the NSSL/CIMMS employees who ensure data collection by KOUN with research-grade quality and John Krause for preparing KOUN data. OU-PRIME is maintained and operated by the Atmospheric Radar Research Center (ARRC) at the University of Oklahoma.

References

Borowska, L., A.V. Ryzhkov, D.S. Zrnić, C. Simmer, R. Palmer, 2011: Attenuation and differential attenuation of the 5-cm wavelength radiation in melting hail. J. Appl. Meteor. Climatol., 50, 59-76

Kaltenboeck R., and Ryzhkov A., 2011: Severe hail size discrimination using dual-polarized weather radar data. A dual-wavelength comparison between C and S band. Extended Abstracts, 6th European Conference on Severe Storms, Palma de Mallorca, Spain, [available online at: http://essl.org/ECSS/2011/programme/abstracts/168.pdf or http://essl.org/ECSS/2011/programme/presentations/168.pdf].

Kaltenboeck R., and Ryzhkov A., 2012: Comparison of polarimetric signatures of hail at S and C bands for different hail sizes. Atmos. Res., submitted

Kumjian, M.R., and A.V. Ryzhkov, 2008: Polarimetric signatures in supercell thunderstorms. J. Appl. Meteor. Climat., 47, 1940-1961

Kumjian, M.R., and A.V. Ryzhkov, 2009: Storm-relative helicity revealed from polarimetric radar observations. J. Atmos. Sci., 66, 667-685

Lemon L., 1998: The Radar ''Three-Body Scatter Spike'': An Operational Large-Hail Signature. Wea. Forecasting, 13, 327-340

Picca, J., and A. Ryzhkov, 2012: A dual-wavelength polarimetric analysis of the 16 May 2010 Oklahoma City extreme hailstorm. Mon. Wea. Rev., 140, 1385 – 1403.

Ryzhkov, A.V., 2007 : The impact of beam broadening on the quality of radar polarimetric data, J. Atmos. Oceanic Technol., 24, No 5, 729–744.

Ryzhkov A., and Zrnić D., 2007: Depolarization in Ice Crystals and Its Effect on Radar Polarimetric Measurements. J. Atmos. Oceanic Technol, 24, 1256-1267

Ryzhkov A., Schuur T., Burgess D., and Zrnic D., 2005a: Polarimetric tornado detection. J. Appl. Meteor., 44, 557-570

Romine G., Burgess D., Wilhelmson R., 2008: A dual-polarization-radar-based assessment of the 8 May 2003 Oklahoma City area tornadic supercell. Mon. Wea. Rev., 136, 2849-2870.;

Straka J., Zrnić D., and Ryzhkov A., 2000: Bulk hydrometeor classification and quantification using multiparameter radar data. Synthesis of relations. J. Appl. Meteor., 39, 1341–1372